Climate Dynamics (2023) 60:3121–3138
https://doi.org/10.1007/s00382-022-06463-2

Response of summer precipitation over the Tibetan Plateau to large tropical volcanic eruptions in the last millennium

Meng Zuo[1] · Tianjun Zhou[1,2] · Wenmin Man[1]

Received: 5 January 2022 / Accepted: 7 August 2022 / Published online: 19 September 2022

Abstract

Changes in summer precipitation over the Tibetan Plateau (TP) significantly influence the surface runoff, river discharge and water availability for the downstream Asian countries, which is sensitive to external forcing. But its response to volcanic eruptions remains unknown. Here we investigate the summer precipitation changes after tropical volcanic eruptions over the TP region by using multiple lines of evidence including reconstructions over the last hundreds of years, observations during recent decades and model simulations covering the last millennium. Both the instrumental data and reconstructions reveal a significant reduction in summer precipitation over the southern TP region during the first summer following tropical volcanic eruptions, which are further confirmed by the coupled model simulations driven by volcanic forcing. The model results indicate that both the dynamic processes related to atmospheric circulation changes and the thermodynamic processes related to specific humidity changes contribute to the decreased precipitation in the southwestern TP, while the thermodynamic process dominates the reduction of precipitation in the southeastern TP. The thermodynamic process results from decreased atmospheric precipitable water caused by decreased surface temperature after tropical volcanic eruptions. The dynamic processes are caused by increased gross moist stability, spatial distribution of surface cooling and a southward shift of westerlies related to weakening and shrinking of Hadley circulation following tropical eruptions. Our results imply that major tropical eruptions have significant impact on the summer precipitation over the southern TP regions, which will further decrease the source of supply for the TP glaciers and runoff output.

Keywords Volcanic eruptions · Summer precipitation · Tibetan Plateau · Dynamics

1 Introduction

The Tibetan Plateau (TP) and its surrounding areas, with an average elevation of more than 4 km, are regarded as the "the Third Pole" (Qiu 2008), which have the largest volumes of ice outside the polar regions (Yao et al. 2007, 2012, 2019). TP is the birthplace of more than 10 major rivers, including the Yellow River, the Yangtze River and the Ganges River, providing water supply to nearly one-sixth of the world's population (Immerzeel et al. 2010). It is thereby called as, the "Water tower of Asia" (Xu et al. 2008). Summer precipitation accounts for more than 70% of the annual total precipitation over most parts of the TP (Ueda et al. 2003; Feng and Zhou 2012; Tong et al. 2014; Ma et al. 2016), which is an important source of supply for the "Asian water tower" glaciers and runoff output (Yao et al. 2012; Zhang et al. 2013). The change in summer precipitation over the TP will not only affect the distribution of water resources but also changes the thermal forcing of TP, further influence the climate over the Northern hemisphere (Duan et al. 2013, 2017). Understanding the response of TP precipitation to both natural and anthropogenic external forcing agents is crucial to climate change adaptation and mitigation activities related to water management and food security (Schewe et al. 2014; Wang et al. 2021; Yao et al. 2022).

As one of the most important natural external forcing, volcanic eruptions inject sulfur gases into the lower stratosphere and convert to sulfate aerosols, resulting in decreased shortwave radiation and global surface temperature, and

✉ Tianjun Zhou
zhoutj@lasg.iap.ac.cn

1 LASG, Institute of Atmospheric Physics, Chinese Academy of Sciences, Beijing 100029, China

2 University of Chinese Academy of Sciences, Beijing 100049, China

have significant impacts on the global hydroclimate (Robock 2000; Timmreck 2012; Zuo et al. 2019). Previous studies reveal decreased global mean precipitation after volcanic eruptions, especially over tropical and monsoon regions (Iles et al. 2013; Barnes et al. 2016; Paik and Min 2017; Zuo et al. 2019), associated with weakened water cycle, decreased surface runoff and freshwater discharge (Grinsted et al. 2007; Trenberth and Dai 2007; Iles and Hegerl 2015; Liu et al. 2018). On a regional scale, the East Asian summer monsoon and South Asian summer monsoon weakened after tropical eruptions in observation and model simulations, associated with decreased precipitation and increased droughts (Anchukaitis et al. 2010; Joshi 2010; Peng et al. 2010; Man and Zhou 2014; Dogar and Sato 2019), which is attributed to the reduction of water vapor, decreased land-sea thermal contrast and the shift of subtropical westerly jet in the upper troposphere (Cui et al. 2014; Man and Zhou 2014). In comparison, less effort has been devoted to the study on the impact of volcanic eruptions on the climate over TP region. Regional mean precipitation over the TP generally decreased after volcanic eruptions based on reconstructions on a decadal time scale (Yang et al. 2014; Liu et al. 2021), and tree-ring records reveal that pre-monsoon droughts on a regional scale are associated with large tropical volcanic eruptions (Liang et al. 2019). Nonetheless, neither the spatial distribution nor the mechanisms of summer precipitation responses were addressed in previous studies.

In this study, we examine the response of summer precipitation over the Tibetan Plateau to large tropical volcanic eruptions during the past millennium by using multiple reconstructions, observations and the Community Earth System Model Last Millennium Ensemble (CESM-LME) simulation, which provides volcanic-only forcing experiments with five ensemble members. We aim to answer the following three questions: (1) What is the summer precipitation response over the TP region following tropical volcanic eruptions based on instrumental data and reconstructions? (2) Can model simulations reproduce the precipitation responses in reconstructions/observations? (3) What are the physical mechanisms of the precipitation anomalies?

The remainder of this paper is organized as follows. Datasets, methods and model simulation are described in Sect. 2. Section 3 presents the summer precipitation responses and physical mechanisms. The conclusions are summarized in Sect. 4.

2 Datasets, methods, and model simulation

2.1 Observations and reconstructions

We use the following datasets, including three gridded reconstructions, two observations and ERA5 reanalysis:

(1) Reconstructed annual May to September precipitation during the period of 1470 to 1999 over the whole Asian continent with a spatial distribution, which is mainly based on 500-year historical documentary records, tree-ring data, ice-core records and long-term instrumental datasets, the horizontal resolution is 0.5°×0.5° (Feng et al. 2013);
(2) Reconstructed May to September precipitation over China derived from 479 tree-ring records, including 371 tree-ring width chronologies, a tree-ring isotope chronology, and 107 drought/flood indices. The dataset covers the period of 1470 to 2000, with a horizontal resolution of 0.5°×0.5° (Shi et al. 2017);
(3) A gridded reconstruction of Asian summer (June-August) precipitation during the period of 1470 to 2013, which is integrated reconstruction of 453 tree-ring-width chronologies and 71 historical documentary records of flood and droughts over the Asian region with a horizontal resolution of 2°×2° (Shi et al. 2018), this dataset provides substantially improved data quality compared with single-proxy-type reconstructions;
(4) The monthly mean precipitation data from the Global Precipitation Climatology Project (GPCP) version 2.2, covering the time period of 1979 to 2010, the horizontal resolution is 2.5°×2.5°. GPCP dataset are produced by merging precipitation estimates computed from microwave, infrared, sounder data observed by the international constellation of precipitation-related satellites, and precipitation gauge analyses, taking advantage of the strengths of each data type (Huffman et al. 2009), which has been widely used in analyzing precipitation changes over TP region (Yao et al. 2012; Hu et al. 2021);
(5) Monthly precipitation data from the Asian Precipitation-Highly Resolved Observational Data Integration Towards Evaluation (APHRODITE), covering the time period of 1951 to 2007, the horizontal resolution is 0.25°×0.25° (Yatagai et al. 2012). APHRODITE is based on rain gauge observations from thousands of Asian stations and those reporting to the World Meteorological Organization (WMO) Global Telecommunications System, which has been widely used and validated to show a better skill in depicting precipitation characteristics in TP region and evaluating Asian water

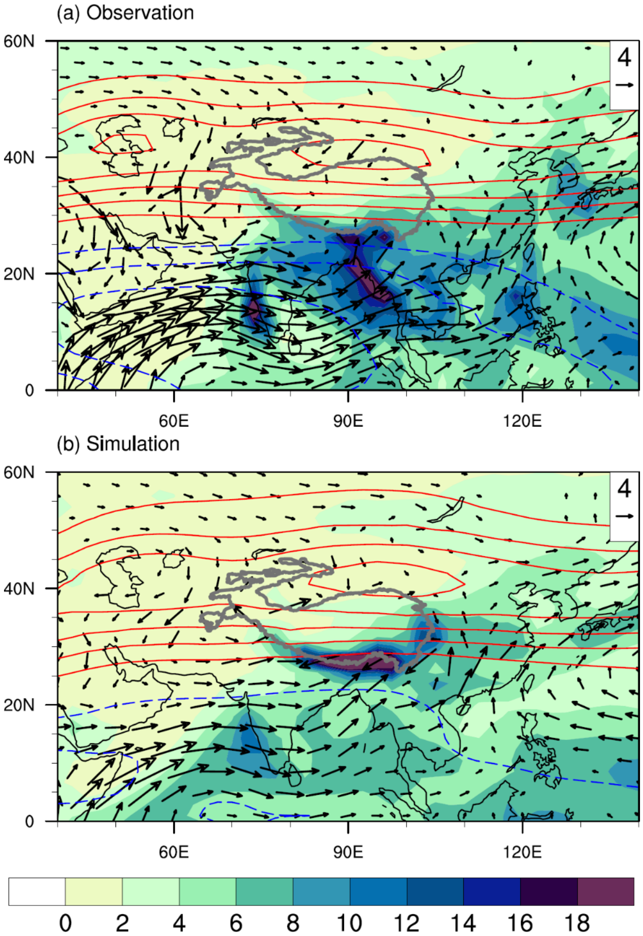

Fig. 1 Comparison of precipitation and circulation climatology (1979–2005) between (a) observation (precipitation from GPCP and circulation from ERA5) and (b) CESM model simulation. The metrics include JJA mean precipitation (mm day^{-1}, shading), 850 hPa wind (m s^{-1}, vector) and 200 hPa zonal wind (m s^{-1}, contour, red for positive value and blue for negative). The solid gray line is the 2000 m elevation contour

resources (Tong et al. 2014; Zhang et al. 2014; Tan et al. 2020).

(6) Wind field of the most advanced reanalysis data ERA5 from the European Centre for Medium Range Weather Forecasts, the horizontal resolution is 0.25°×0.25° (Hersbach et al. 2020).

2.2 Model simulations

The volcanic-only forcing experiments in CESM-LME simulations are used to reveal the model results and physical mechanisms. CESM-LME employs the version 1.1 of CESM with the Community Atmosphere Model version 5 (CAM5) (Hurrell et al. 2013; Otto-Bliesner et al. 2016). The horizontal resolution of atmosphere and land components is ~2°, the ocean and ice components utilize a resolution of ~1°. The simulations cover the time period of 850 to 2005, during which the main external forcings are orbital forcing, solar insolation, volcanic eruptions, land use, greenhouse gases and ozone-aerosol forcing (after 1850). CESM-LME has five-member volcanic-only forcing experiments, which use the volcanic activity reconstruction of Gao et al. (2008). The estimated volcanic aerosol loadings are prescribed as a fixed single size distribution in the model. Details can be found in Otto-Bliesner et al. (2016).

Following the previous studies, we calculate the multi-member mean of five-member volcanic-only forcing experiments to remove the impact of internal variability as much as possible (Zuo et al. 2018, 2019). Before examining the simulated response to volcanic eruptions, we firstly evaluate the model performances in simulating the climatology of summer precipitation and circulation over the TP region. We used the monthly mean precipitation data from the GPCP and monthly mean circulation data from ERA5 as previous studies did (Sperber et al. 2013; Fiedler et al. 2020; Ding et al. 2021). Compared with observations, we found that CESM-LME simulations can reasonably reproduce the climatological summer precipitation and circulation over the TP (Fig. 1). Previous studies also reveal that CESM-LME can well simulate the climate response to volcanic eruptions (Stevenson et al. 2016; Zuo et al. 2019, 2021).

2.3 Selection of volcanic eruptions

We select tropical volcanic eruptions from observations, reconstructions and CESM-LME simulations. For the APHRODITE (since 1951) and GPCP (since 1979) datasets, we select all low-latitude eruptions with intensity greater than 10 Tg[H_2SO_4] to including more events (Table 1), and this threshold is enough to get a robust climate response to volcanic eruption (Man et al. 2014). For reconstructions and model simulations covering longer time periods, we select the tropical eruptions according to the reconstructed volcanic aerosol loadings (Gao et al. 2008; Stevenson et al. 2016). The ratio between Northern and Southern Hemisphere stratospheric aerosol loading can be used to classify the location of volcanic eruptions. Following the threshold in Stevenson et al. (2016) and Zuo et al. (2019), ratios between 0.7 and 1.3 are tropical eruptions. And we used a higher threshold of 20 Tg sulphate aerosol to get a robust hydroclimate response to volcanic eruption beyond the influence of internal variability (Zhuo et al. 2014; Azoulay et al. 2021; D'Agostino and Timmreck 2022) (Table 1).

2.4 Superposed epoch analysis

We apply the superposed epoch analysis (SEA) method (Haurwitz and Brier 1981) to examine the summer precipitation changes over TP region in the selected volcanic

Table 1 List of eruption years for large tropical volcanic eruptions in the observations, reconstructions and CESM-LME simulation

Datasets	Eruption years
Observation (APHRODITE)	1963 (Mount Agung), 1982 (Mount El Chichón), 1991 (Mount Pinatubo)
Observation (GPCP)	1982, 1991
Reconstruction (Feng et al. 2013)	1815 (Mount Tambora), 1883 (Mount Krakatau), 1991
Reconstruction (Shi et al. 2017)	1815, 1883, 1991
Reconstruction (Shi et al. 2018)	1815, 1883, 1991
CESM-LME	1001, 1258, 1284, 1815, 1883, 1991

eruption years to investigate the temporal response to the tropical volcanic eruptions. We select a 14-year window for the composite. Year 0 is regarded as the time volcanic aerosol loadings reach its peak. Anomalies are calculated relative to 5-year mean before the volcanic eruptions (Fischer et al. 2007; Iles et al. 2013; Zuo et al. 2019). We construct a Monte Carlo Model (Adams et al. 2003) to test the statistical significance of the precipitation response. The SEA results reveal a most significant response during year 1, therefore this study focuses on the precipitation response in the first boreal summer (June-July-August).

2.5 Moisture budget analysis

Moisture budget analysis is used to decompose the precipitation into changes in evaporation and moisture advection. Here we apply the moisture budget analysis to reveal the physical processes related to summer precipitation changes over the TP region after tropical volcanic eruptions (Chou et al. 2009; Zuo et al. 2019).

On the interannual time scale, the precipitation anomalies can be decomposed as the following formula:

$$P' = - < \omega \partial_p q >' - < \mathbf{V} \bullet \nabla q >' + E' + residual \quad (1)$$

P and E are precipitation and evaporation, respectively. ω and $\mathbf{V}$ represent vertical velocity and horizontal winds in pressure level coordinates, respectively. q is specific humidity. The primes $'$ denote the response to volcanic eruptions, and brackets < > is the mass-weighted vertical integrals from the bottom to top of the troposphere. In this equation, precipitation changes are decomposed into changes in evaporation, vertical moisture advection $< \omega \partial_p q >'$ and horizontal moisture advection $< V_h \bullet \nabla \mathrm{q} >'$. The moisture advection terms can be further divided into thermodynamic terms associated with specific humidity changes and dynamic terms related to circulation changes. The formula is rewritten as:

$$P' = E' - < \overline{\omega} \partial_p q' > - < \omega' \partial_p \overline{q} > - < \overline{\boldsymbol{V}_h} \bullet \nabla \mathrm{q}' > - < \boldsymbol{V}'_h \bullet \nabla \bar{q} > + NL \quad (2)$$

Where the NL represents a sum of nonlinear terms.

2.6 Moist static energy budget analysis

The moisture budget analysis can attribute precipitation anomalies to changes in vertical motion, however, we need to apply the moist static energy budget to further reveal the mechanism of changes in vertical motion. According to Neelin and Held (1987), vertical motion in the deep convection regions is determined by the column-integrated moist static energy (MSE) budget. The MSE equation is derived from combining the vertically integrated thermodynamic equation and moisture equation (Neelin, 2007), written as:

$$\partial_t < C_p T + L_v q >' + < \boldsymbol{V} \bullet \nabla_h (C_p T + L_v q) >' + < \omega \partial_p h >' = F'_{net} \quad (3)$$

Among which the MSE (h) is the sum of moist enthalpy ($C_p T + L_v q$) and geopotential height (ϕ). C_p is specific heat at constant pressure and L_v denotes latent heat of vaporization; T and q are air temperature and specific humidity, respectively. $\boldsymbol{V}$ and ω are horizontal winds and vertical velocity in pressure level coordinates, respectively. F_{net} is the net MSE flux in the atmospheric column, which can be expressed as $F_{net} = F_t - F_s$. The subscript $_t$ and $_s$ represent top and surface of the atmosphere, respectively. The net MSE flux at the TOA $F_t = S_t^{\downarrow} - S_t^{\uparrow} - R_t^{\uparrow}$, and the net MSE flux at the surface $F_s = S_s^{\downarrow} - S_s^{\uparrow} + R_s^{\downarrow} - R_s^{\uparrow} - LH - SH$, with S and R represent shortwave and longwave radiation, LH and SH are latent heat flux and sensible heat flux, respectively.

Similar to the moisture budget analysis, the MSE equation can be rewritten as:

$$< \omega' \partial_p \overline{h} > \approx F'_{net} - < \overline{\boldsymbol{V}} \bullet \nabla_h (C_p T + L_v q)' >$$

$$- < \boldsymbol{V}' \bullet \nabla_h \overline{(C_p T + L_v q)} > - < \overline{\omega} \partial_p h' > + NL \quad (4)$$

Vertical advections of climatological MSE ($< \omega' \partial_p \overline{h} >$) is balanced by the net heat flux F'_{net}, horizontal moist enthalpy advection and vertical MSE advection by climatological vertical motion $< \overline{\omega} \partial_p h' >$. NL is the sum of nonlinear terms. The reduced (increased) MSE associated with physical processes on the right-hand side of the Eq. (4) would result in descending (ascending) motions, to keep the balance of MSE budget (Back and Bretherton 2009; Wu et al. 2017; Zuo et al. 2019).

3 Results

3.1 Summer precipitation responses over TP in observations and reconstructions

To reveal the response of summer precipitation to tropical volcanic eruptions over TP regions, we firstly use the observational precipitation datasets from APHRODITE and GPCP. We firstly select all low-latitude eruptions with intensity greater than 10 Tg[H_2SO_4] (Table 1). Since APHRODITE and GPCP overlap on two volcanic eruptions (the Mount El Chichón in 1982 and the Mount Pinatubo in 1991), we examine the precipitation response to these two eruptions. Similar results are obtained after taking the Mount Agung in 1963 into consideration based on APHRODITE (Fig. S1). The superposed epoch analysis results reveal a significant decreased summer precipitation over the southern TP region in the first year following major tropical eruptions (Fig. 2), decreased by over 1 mm day^{-1} on a regional scale, which is about 16.7% of climate mean value. Due to the small sample of observed volcanic eruptions, we further examine the warm season precipitation anomalies after tropical volcanic eruptions based on gridded long-term reconstructions over the past 530 years. We found an overall deficient rainfall over the southern TP region after large tropical volcanic eruptions in three sets of reconstruction (Fig. 3). The above results suggest that the summer precipitation over southern TP region tends to decrease after tropical volcanic eruptions based on historical records and observations.

3.2 Summer precipitation responses over TP in CESM-LME simulation

We further analyze the summer precipitation responses over TP to volcanic eruptions during the last millennium based on the volcanic-only forcing experiment in CESM-LME simulation. The decreased precipitation is further demonstrated by model simulations (Fig. 4a). A decrease of precipitation with an intensity of 1.2 mm day^{-1} is seen over southwestern TP in the SEA result, which is consistent with observations (Fig. 2). Quantitatively, the average precipitation over southern TP region decreased by 0.7 mm day^{-1} (about 9% of summer mean climatology) in the first summer following tropical volcanic eruptions (Fig. 4b). We further extend our analysis to surface runoff based on CESM-LME (Fig. S2). A significant decrease in surface runoff appears during the first summer after tropical volcanic eruptions, which shows similar spatial distribution with precipitation response. Regional mean surface runoff over southern TP decreased by ~6.4% relative to the climatological mean, indicating an important impact of tropical volcanic eruptions on the potential water resources.

3.3 Physical mechanism underlying the precipitation response

Both observations and model simulations reveal a significant decreased precipitation over the southern TP region. We examine the underlying physical mechanisms by using the moisture budget analysis (Chou et al. 2009) and MSE budget analysis (Neelin and Held 1987).

We firstly present the results of moisture budget for the regional mean precipitation response over the southern TP in CESM-LME (Fig. 5a). The decreased precipitation over the southern TP region is mainly contributed by the anomalous negative vertical moisture advection $-<\omega\partial_p q>'$ (Fig. 5a). We further divide this term into the anomalous vertical moisture advection by climatological vertical motion $-<\overline{\omega}\partial_p q'>$ (thermodynamic term) and the anomalous advection of the climatological moisture by vertical motion anomalies $-<\omega'\partial_p\overline{q}>$ (dynamic term) (Fig. 5b-c). We found that both thermodynamic and dynamic terms contribute to the precipitation reduction, and their relative contributions are different in the southwestern and southeastern TP region. Therefore, we divided the southern TP into southwest and southeast regions. The regional mean results show that both the dynamic and thermodynamic processes contribute to the decreased precipitation in the SouthWest region of TP, while the changes in thermodynamic process dominates the reduction of precipitation in the SouthEast region of TP (Fig. 5d).

What are the physical processes that dominate the changes in thermodynamic term $-<\overline{\omega}\partial_p q'>$? We show the climatology of summer mean atmospheric precipitable water with vertically integrated moisture flux (Fig. 6a). During boreal summer, the water vapor of TP mainly comes from the Bay of Bengal, Arabian Sea, the South China Sea, and the mid-latitudes (Fig. 6a). In the first summer after the tropical eruptions, there is a significant decrease of atmospheric precipitable water over the southern TP region as a result of cooler global temperature induced by tropical volcanic eruptions, which corresponds to the decreased water vapor transport from the western and southern boundaries of the TP (Fig. 6b). The spatial distribution of the anomalous water vapor transport is consistent with the lower atmospheric circulation, features a weakened South Asian and East Asian summer monsoon. The resulted northwesterly anomalies in the south of TP reduce the water vapor transport into the TP (Fig. 6b).

What are the processes that determine the changes in dynamic term $-<\omega'\partial_p\overline{q}>$? The spatial distribution of the summer vertical pressure velocity anomalies during

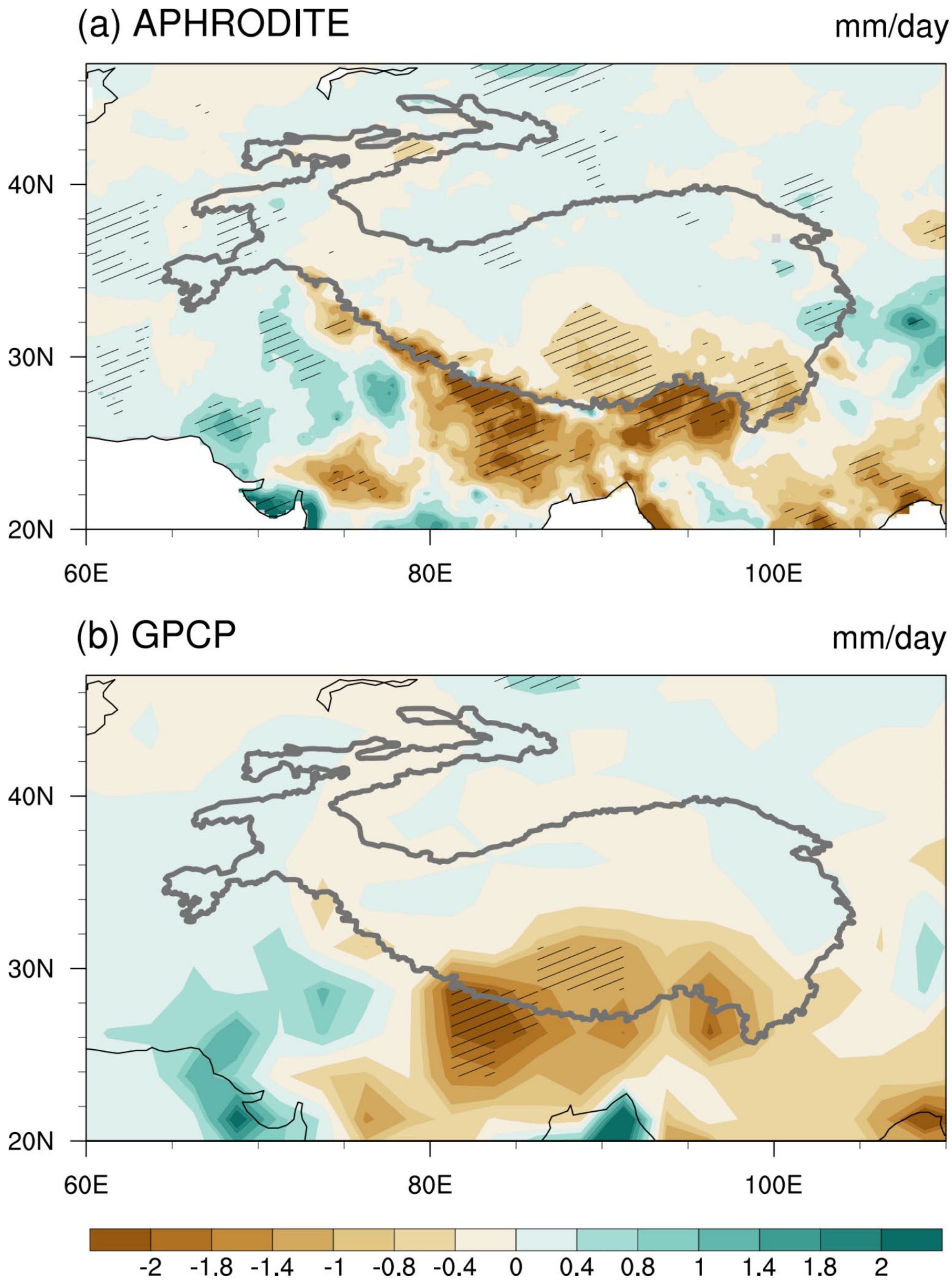

Fig. 2 Precipitation (mm day^{-1}) anomalies in the first boreal summer (JJA) over the Tibetan Plateau (TP) following large tropical volcanic eruptions based on the (a) APHRODITE dataset and (b) GPCP dataset. Slashes indicate values $\geq$ 90% confidence level based on the Monte Carlo test (n = 10,000). The solid gray line is the 2000 m elevation contour

the first year after tropical volcanic eruptions is shown in Fig. 7a, which is consistent with the dynamic term in Fig. 5c, indicating that the decreased summer precipitation in the SouthWest region of TP is caused by the descending anomalies. We further examine the sources of descending anomalies over the SouthWest region of TP by using the MSE budget analysis. In the southern TP region, the vertical motions are constrained by the MSE budget balance. The descending anomalies tend to decrease MSE exported out of the atmospheric column, leading to positive vertical advections of the climatological MSE ($- < \omega'\partial_p\overline{h} >$). Our budget analysis indicates that this term is mainly caused by the negative vertical MSE advection by the climatological vertical motion ($- < \overline{\omega}\partial_p h' >$), negative horizontal advection of anomalous dry enthalpy by climatological wind $- < \overline{\boldsymbol{V}} \bullet \nabla_h (C_pT)' >$ and negative horizontal advection of climatological moist enthalpy by anomalous wind $- < \boldsymbol{V'} \bullet \nabla_h \overline{(L_vq)} >$ (Fig. 7b), while other terms results in ascending anomalies.

The term $- < \overline{\omega}\partial_p h' >$ is associated with the vertical structure of anomalous MSE (h'), which is manifested in the gross moist stability change. Figure 7c shows the vertical profiles of regional mean h' over the SouthWest region of TP and its sub components dry static energy $s_{,} = C_pT' + \phi'$

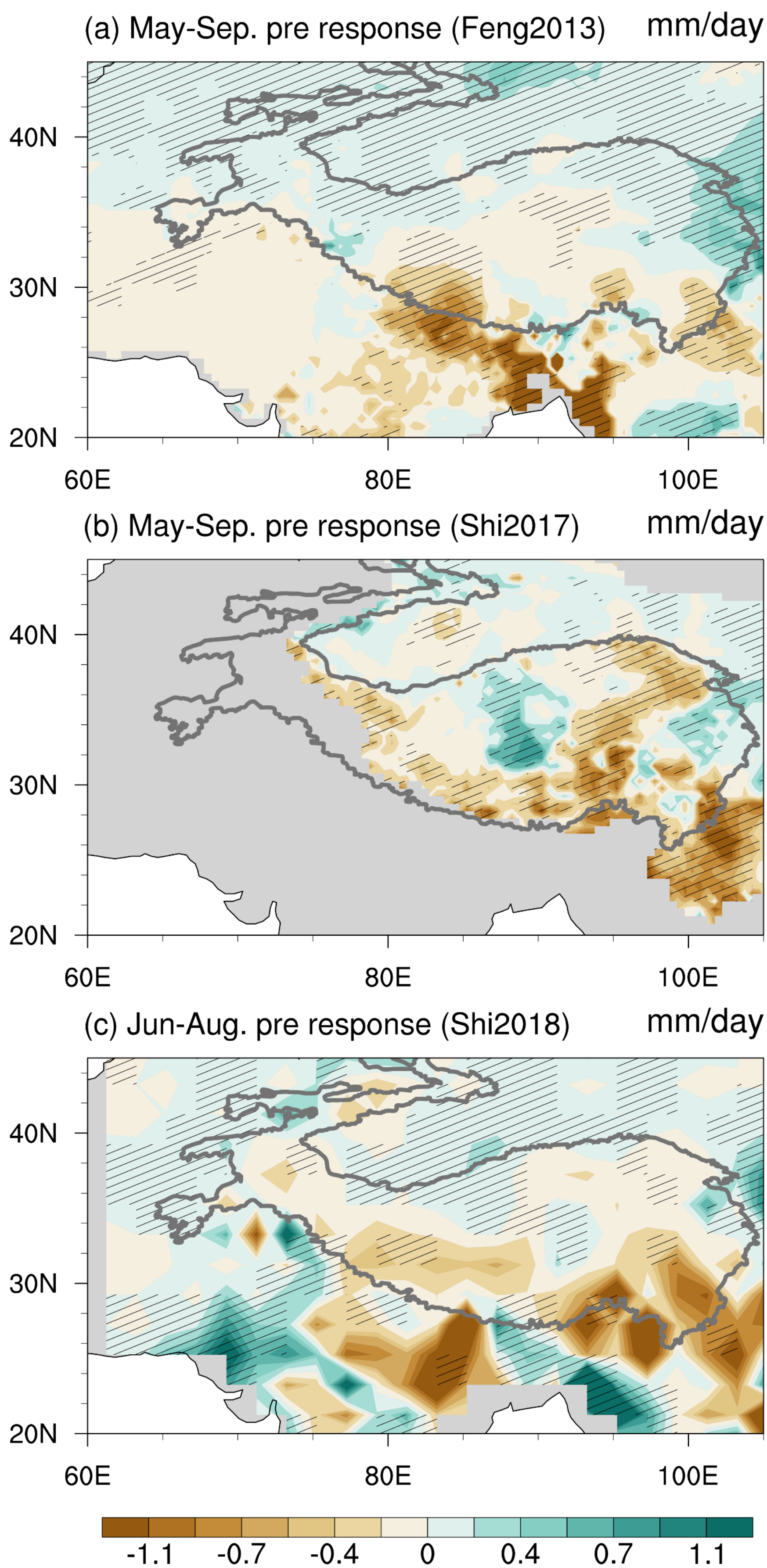

Fig. 3 Reconstructed precipitation anomalies in the first boreal summer over the TP following large tropical volcanic eruptions based on the reconstructed (a) warm season precipitation (mm day^{-1}) by Feng et al. (2013), the reconstructed (b) May-September precipitation (mm day^{-1}) over China by Shi et al. (2017) and the reconstructed (c) June-August precipitation (mm day^{-1}) over Asia by Shi et al. (2018). Slashes indicate values $\gtrsim$ 90% confidence level based on the Monte Carlo test (n = 10,000)

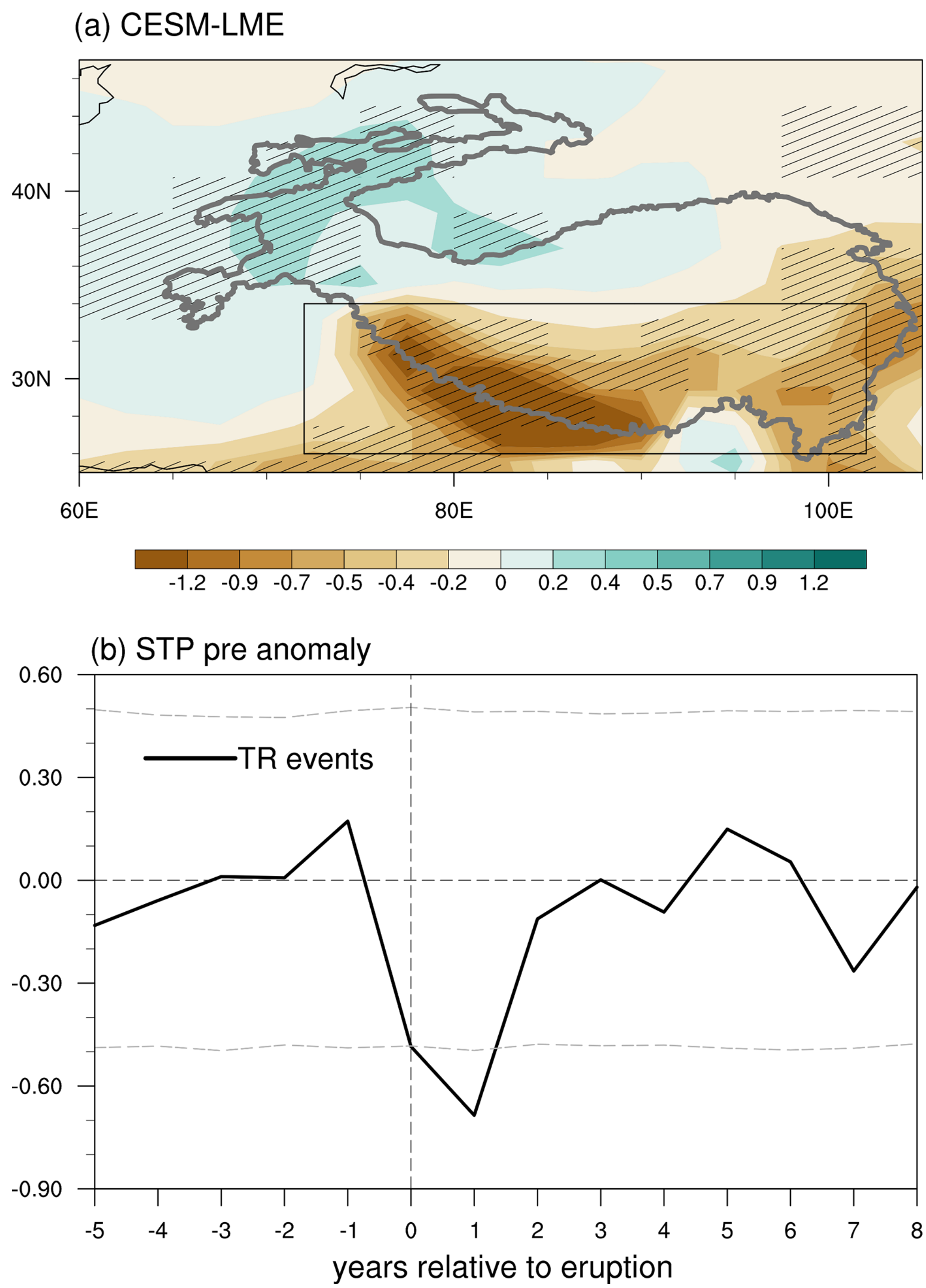

Fig. 4 (a) Precipitation anomalies (mm day^{-1}) in the first boreal summer over the TP following large tropical volcanic eruptions based on the CESM-LME simulation. Slashes indicate values $\geq$ 95% confidence level based on the Monte Carlo test (n = 10,000). (b) Superposed epoch analysis (SEA) of summer precipitation changes over the southern TP region (26–34°N, 72–102°E) after large tropical volcanic eruptions (TR events) (units: mm day^{-1}). The anomalies are calculated relative to a 5-year pre-eruption mean. Gray dashed lines represent confidence intervals of 95% derived from 10,000 Monte Carlo simulations

and latent energy $L_v q'$, we found an increased gross moist stability after volcanic eruptions induced by decreased MSE in the lower to middle troposphere and increased MSE in the upper troposphere to lower stratosphere. The vertical structure of h' in the lower to middle troposphere is dominated by the changes in latent energy $L_v q'$, with larger negative anomaly in the lower to middle troposphere than that in the upper troposphere; and the h' higher than 200 hPa is dominated by the $s_{\prime}$, with a positive anomaly caused by stratospheric warming, resulting in an increased gross moist stability $-<\overline{\omega}\partial_p h'>$ and descending anomalies, which suppress the local convection over the SouthWest region of TP.

The terms $-<\overline{\boldsymbol{V}}\bullet\nabla_h(C_pT)'>$ and $-<\boldsymbol{V}'\bullet\nabla_h\overline{(L_vq)}>$ can be further divided into zonal and meridional components (Fig. 8). We found that the negative zonal components $-<\overline{u}\bullet\partial_x(C_pT)'>$ and $-<u'\bullet\partial_x\overline{(L_vq)}>$ over the SouthWest region of TP play a dominant role, with the largest response at 400 hPa (Figures not shown). As for the negative anomaly of

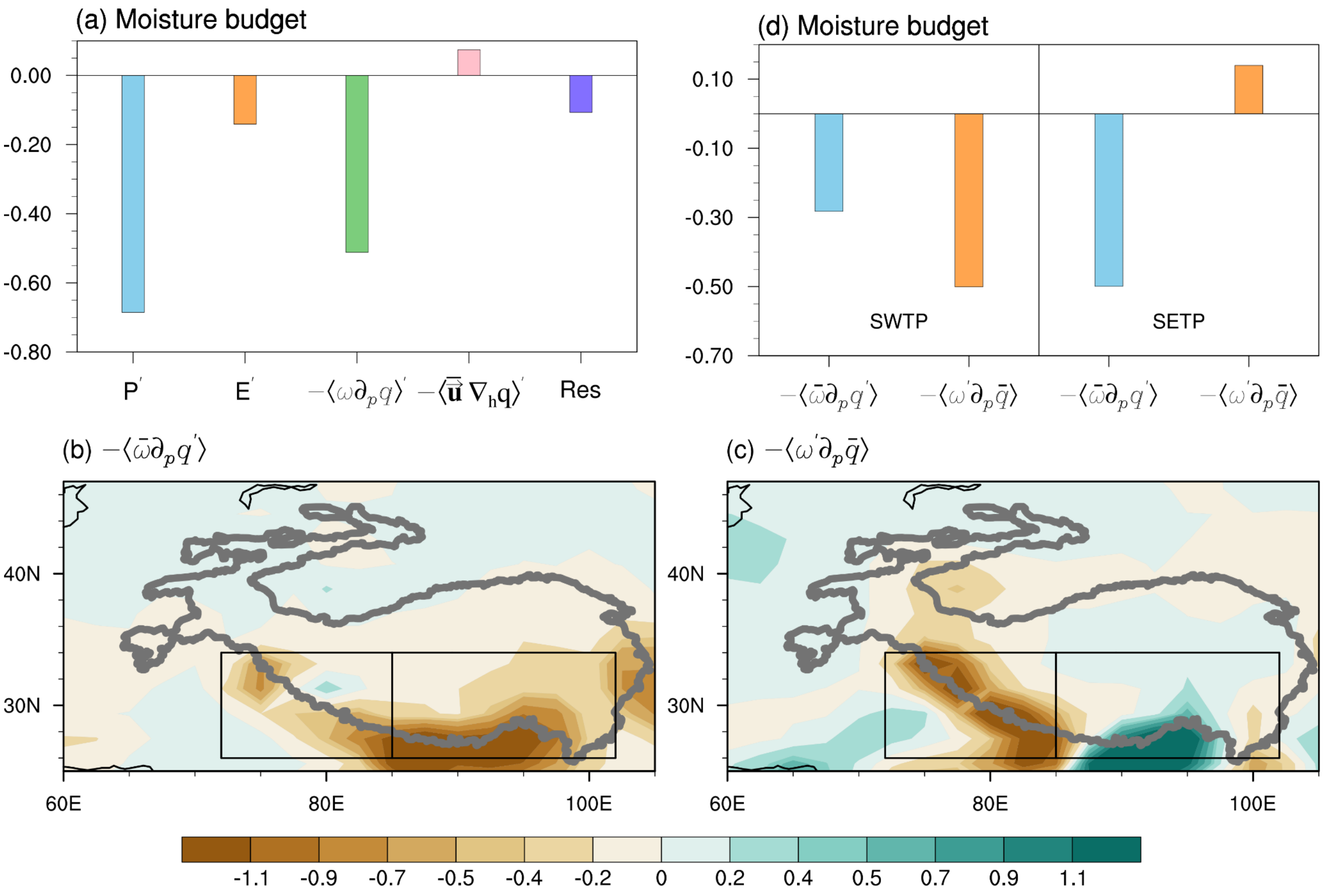

Fig. 5 (a) Moisture budget for regional mean precipitation anomaly (mm day^{-1}) over the southern TP region following tropical volcanic eruptions based on CESM-LME simulations. Spatial distribution of (b) anomalous vertical moisture advection by climatological vertical motion (thermodynamic term) and (c) anomalous advection of the climatological vertical moisture by vertical motion anomalies (dynamic term). (d) Decomposition of anomalous vertical moisture advection over the southwestern TP (SWTP, 26–34°N, 72–85°E) and southeastern TP regions (SETP, 26–34°N, 85–102°E) (mm day^{-1})

$- < \overline{u} \bullet \partial_x (C_p T)' >$, we examine the summer air temperature anomalies during the first year following tropical volcanic eruptions with the climatological summer wind filed at 400 hPa (Fig. 9a). There is a stronger cooling over the west side of TP after the tropical eruptions, and the climatological westerlies will transport the air with lower dry static energy to the TP region, the anomalous dry enthalpy by the zonal wind reduces the moist enthalpy into the air column, resulting in the descending anomalies (Fig. 9a). To find out the cause of negative anomaly of $- < u' \bullet \partial_x \overline{(L_v q)} >$, we show the climatological summer mean specific humidity with wind anomalies at 400 hPa (Fig. 9b). There is a center of large climatological specific humidity in the southern TP region. Following the tropical volcanic eruptions, the westerly anomalies on the south of TP associated with the anomalous cyclonic circulation, bring the air with low moist enthalpy into the southern TP region, forming the descending anomalies (Fig. 9b). To determine the mechanisms for the changes in westerlies, we show the response of westerlies at 400 hPa to tropical eruptions (Fig. 10b). The center of climatological westerlies locates in around 40°N (Fig. 10a), and there is a significant southward shift of westerlies after tropical eruptions (Fig. 10b). We further examine the zonal mean and regional Hadley circulation response over the southern TP region (70–120°E) based on method used in D'Agostino and Timmreck (2022). The results show that the zonal mean Hadley circulation weakens and shrinks during the first summer after eruptions (Fig. 10c), and the local Hadley circulation over the South Asian monsoon region show larger anomaly (Fig. 10d). The weakened local Hadley circulation is induced by reduced atmospheric net energy input and the increased gross moist stability at the updraft branch, as less MSE exported from the ITCZ (Fig. S3), which is consistent with study of D'Agostino and Timmreck (2022). Therefore, the southward shift of westerlies can be seen as a shrinking and weakening of Hadley circulation.

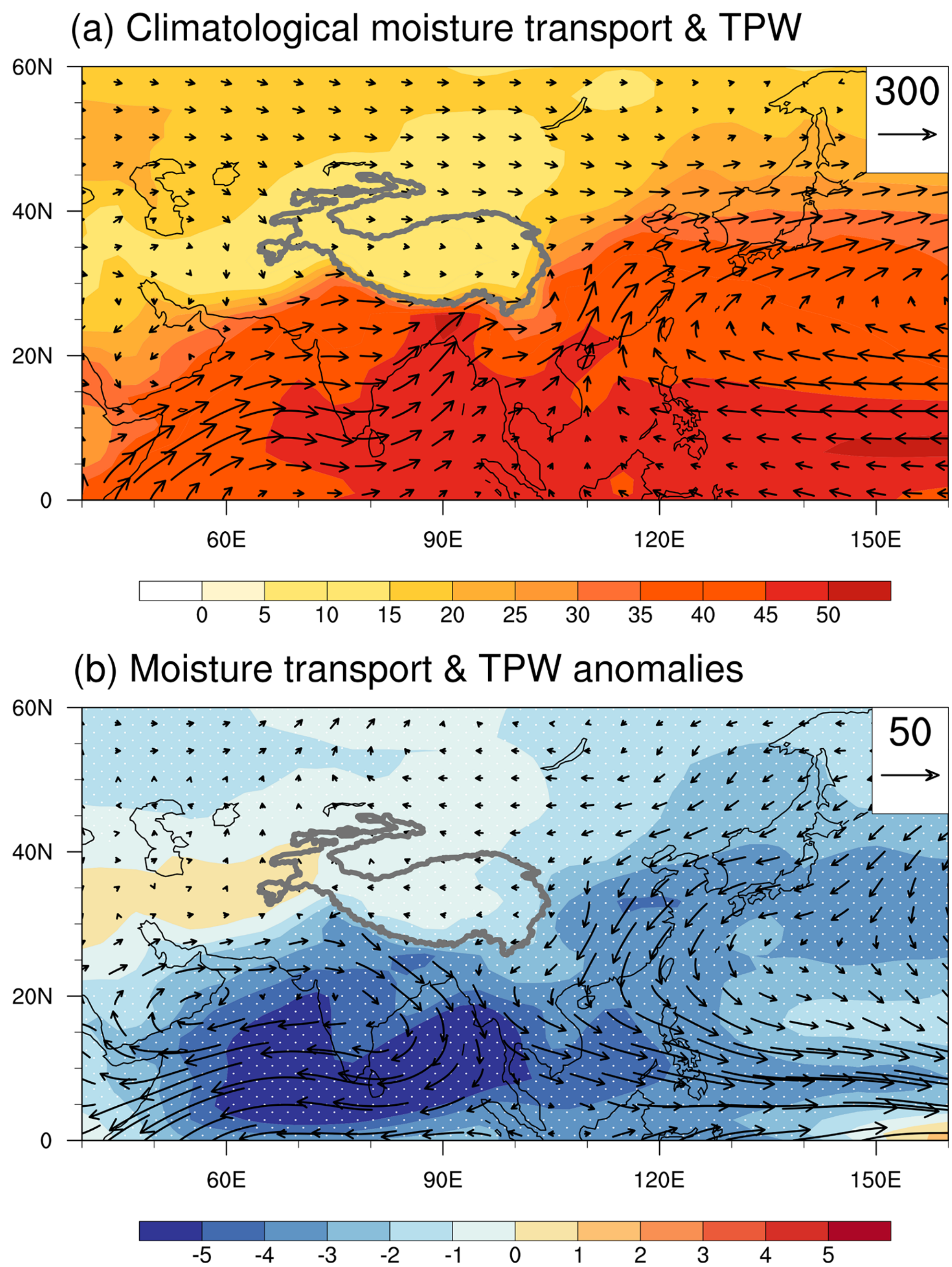

Fig. 6 (a) The climatological JJA mean total atmospheric precipitable water (TPW) (shading, kg m^{-2}) with vertically integrated moisture flux (vector, kg m s^{-1}) derived from CESM-LME simulations. (b) As in (a), but for the anomalies in the first JJA after tropical volcanic eruptions. Dots indicate values $\gtrsim$ 95% confidence level based on the Monte Carlo test (n = 10,000)

4 Discussion

Since usually El-Niño occurs after strong volcanic eruptions (Ward et al. 2021), in both observations and reconstructions, the volcanic signal is super-imposed on interannual variability in specific events. Previous studies revealed an El Niño-like SST response to tropical volcanic eruptions based on multi-model mean results (Stevenson et al. 2016; Predybaylo et al. 2017; Zuo et al. 2018; Ward et al. 2021), with different responses among the models (Ding et al. 2014; Maher et al. 2015; Chai et al. 2020). Given the superposition of tropical volcanic eruption and El Niño, which is also known to have large impact on TP precipitation (Hu et al. 2021), we further examined their relative influence on precipitation in the SouthWest region of TP. To reveal the relative impact of ENSO response to precipitation anomalies over the SouthWest region of TP, we firstly examine the relationship between Niño3.4 index anomalies and the precipitation anomalies over the SouthWest region of TP based on the selected 30 volcanic samples (6 volcanic eruptions in each member) in CESM-LME. Although the ensemble mean response of Niño3.4 index is positive, there is still large spread between each sample, which means La Niña-like SST anomalies are associated with some

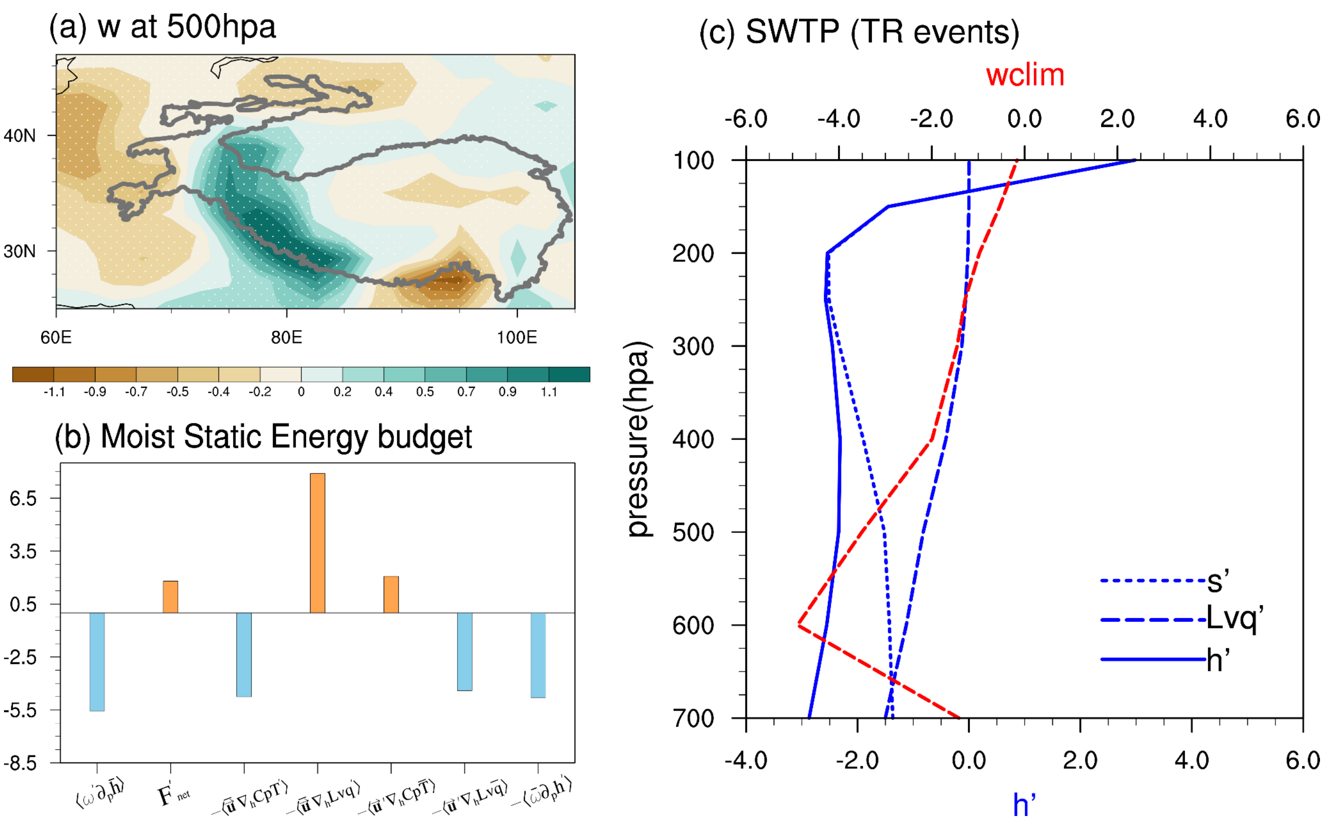

Fig. 7 (a) Spatial distribution of the JJA mean vertical pressure velocity anomalies (shading, multiplied by 80; Pa s^{-1}) during the first year after tropical volcanic eruptions based on CESM-LME simulations. Dots indicate values $\geq$ 95% confidence level based on the Monte Carlo test (n = 10,000). (b) Moist static energy budget for the southwestern TP (SWTP) regions (26–34°N, 72–85°E) with anomalous descending flows (units: W m^{-2}). (c) Vertical profiles of climatological vertical velocity in pressure level coordinates (wclim, red line; 10^{-2} Pa s^{-1}) and anomalous MSE (blue solid line), dry static energy ($s' = C_pT' + \phi'$, blue dotted line), and latent energy (L_vq'; blue dashed line, kJ kg^{-1}) averaged over the southwestern TP (SWTP) region following tropical volcanic eruptions

volcanic eruptions. We found a significant negative correlation of −0.53 (Fig. S4), indicating that the precipitation in the SouthWest region of TP decreased more when there is an El Niño-like SST response in the first summer after tropical volcanic eruptions.

Based on the preindustrial control (Picontrol) experiment, Figs. S4b-c show the summer precipitation anomalies associated with El Niño and La Niña without external forcing. The El Niño (La Niña) corresponds to decreased (increased) precipitation over the SouthWest region of TP, which will modulate the precipitation responses to tropical volcanic eruptions. We further divide the precipitation anomalies into ENSO-induced changes and direct response based on a statistical method (Pausata and Camargo 2019; Zuo et al. 2021). We select the ENSO events in the Picontrol experiment, which has the same intensity and evolution characteristics with that in the volcanic-forcing simulations based on Niño3.4 index, and construct the composite of ENSO-induced changes. After subtracting the ENSO-induced changes from the total precipitation response, the direct response is obtained. The results show that with El Niño-like SST anomaly in summer of year 1, both the SST response and direct response contribute to the decreased precipitation over the SouthWest region of TP, leading to a stronger precipitation response, among which the ENSO-induced changes account for 55% (Fig. S4d). When a La Niña-like SST response occurs in the summer of year 1, the direct response results in decreased precipitation over the SouthWest region of TP, which is offset by the SST response, resulting in an overall weak response (Fig. S4d).

We also acknowledge the model biases in simulating the precipitation over TP and the surrounding regions in our study. Although the maximum center is reasonably captured over the southern slope of the TP, the Western Ghats and the Burmese coast, the model underestimates the precipitation intensity over the Western Ghats and the Burmese coast, while overestimates the precipitation over the southern slope of the TP and the Indo-Gangetic Plain. Misrepresentation of a number of physical processes has been proposed to account for the precipitation biases over South Asia, including deficiencies in the convective parameterization in the atmospheric model (Bollasina and Ming, 2013), biases in

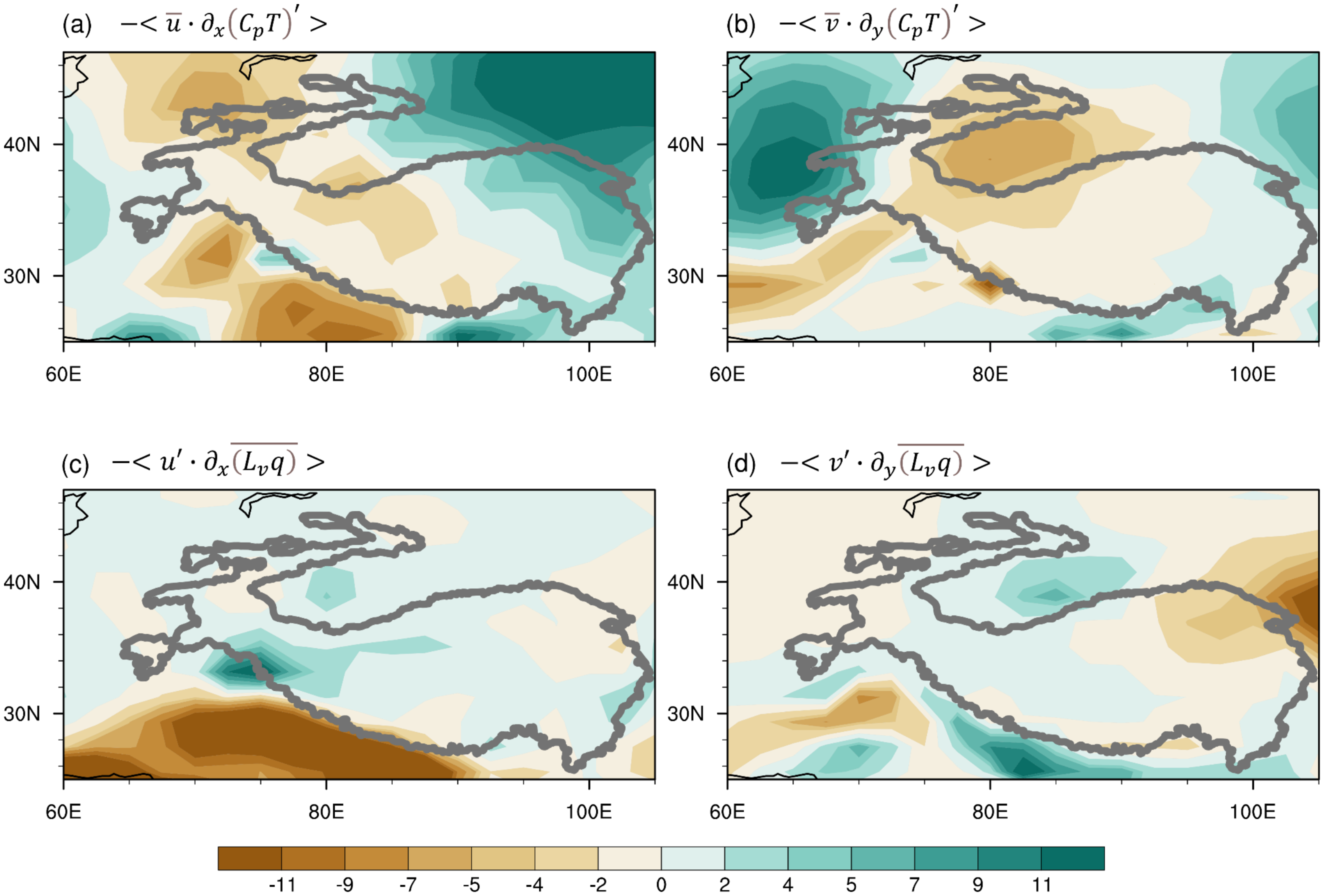

Fig. 8 Spatial distribution of the decomposition of the horizontal advection of anomalous dry enthalpy by climatological wind ($-<\overline{\boldsymbol{u}}\bullet\nabla_h(C_pT)'>$) and horizontal advection of climatological moist enthalpy by anomalous wind ($-<\boldsymbol{u}'\bullet\nabla_h\overline{(L_vq)}>$) based on CESM-LME simulations. (a) $-<\overline{u}\bullet\partial_x(C_pT)'>$, (b) $-<\overline{v}\bullet\partial_y(C_pT)'>$, (c) $-<u'\bullet\partial_x\overline{(L_vq)}>$ and (d) $-<v'\bullet\partial_y\overline{(L_vq)}>$ (W m^{-2})

air-sea interaction and wind stress in the Indian Ocean (Bollasina and Nigam 2009; Annamalai et al. 2017), cold sea surface temperature bias in the northern Arabian Sea (Izumo et al. 2008; Levine et al. 2012), coarse spatial resolution (Xie et al. 2006; Acosta and Huber 2017; Anand et al. 2018) and smoothed representation of topography (Boos and Hurley 2013). Accurately simulating the precipitation over the TP region is also a great challenge for current climate models because of the complex topography. Most models show a positive bias in simulating the TP precipitation (Su et al. 2013; Zhu et al. 2020). The excessive precipitation over the southern slope of TP is likely caused by too strong orographic diabatic heating (O'Brien et al. 2013) and the poor representation of topography (Anand et al. 2018). Using finer topography improves the simulated precipitation distribution over the TP (Li et al. 2015), but high-resolution regional models still overestimate the precipitation over the TP, which is partly related to the deep convection parameterization scheme in models (Gu et al. 2020; Li et al. 2021). Further analysis based on models with higher resolution or regional climate models with better performances in TP precipitation is needed in the future.

5 Summary

Changes in summer precipitation over the Tibetan Plateau (TP) significantly influence the water resources for the "Asian water tower". The sensitivity of TP precipitation to anthropogenic external forcing agents are well addressed, while less effort was devoted to natural external forcing such as volcanic aerosols. In the past millennium, more than 20 volcanoes that have world-wide climate influence have occurred. But how the TP precipitation response to volcanic eruptions remains unknown. In this study, we investigate the summer precipitation changes after tropical volcanic eruptions over the TP region by using multiple lines of evidences including reconstructions, observations and coupled model simulations. Three sets of reconstructions with spatial distribution, observations with high resolution are used

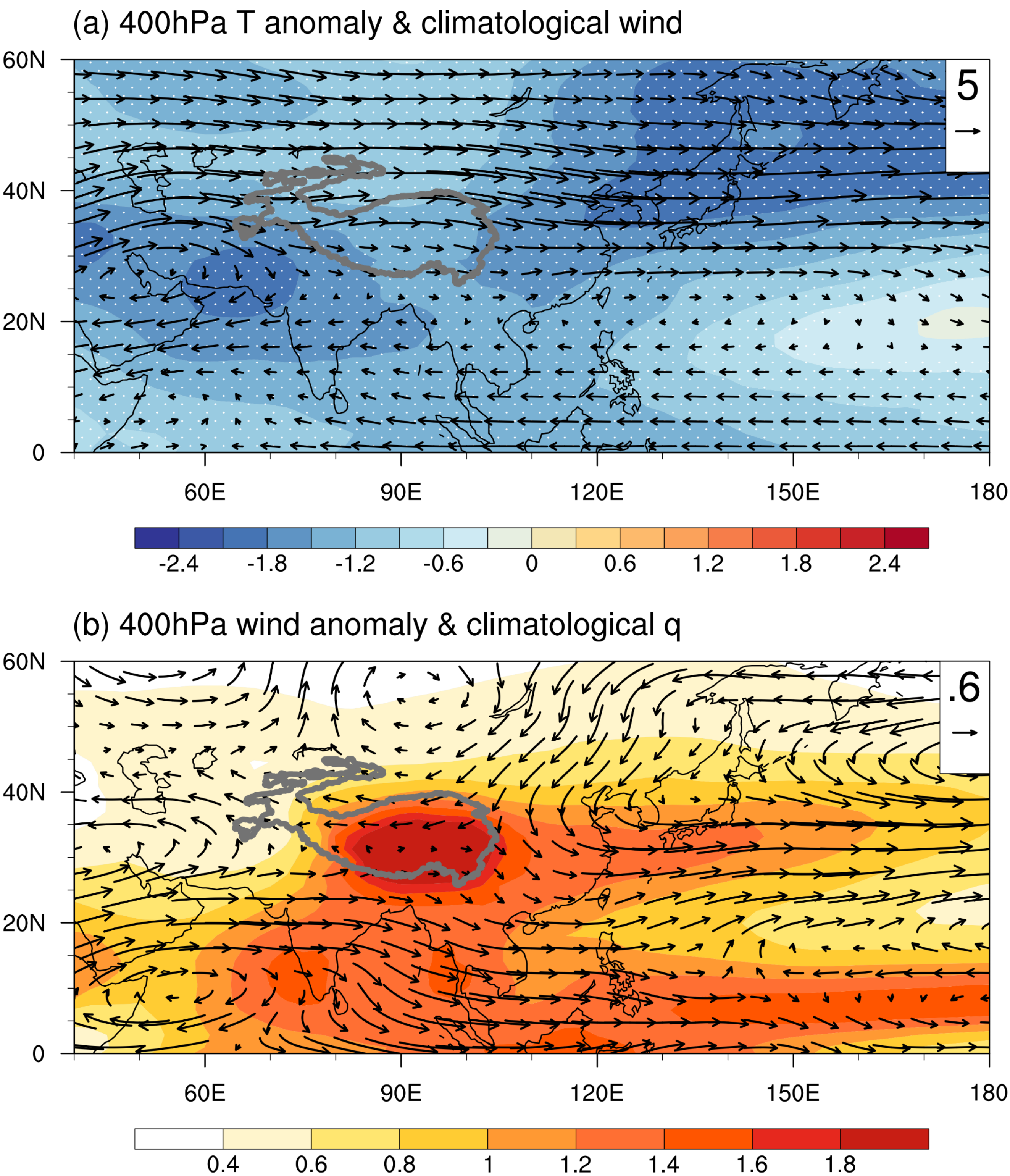

Fig. 9 (a) The JJA mean air temperature anomalies at 400 hPa (shading, K) during the first year following tropical volcanic eruptions with the climatological JJA mean wind at 400 hPa (vector, m s^{-1}) derived from CESM-LME simulations. Dots indicate values $\geq$ 95% confidence level based on the Monte Carlo test (n = 10,000). (b) The climatological JJA mean specific humidity at 400 hPa (shading, g kg^{-1}) with 400 hPa wind anomalies (vector, m s^{-1})

to reveal the precipitation responses. The volcanic forcing simulations over the last millennium are used to reveal the

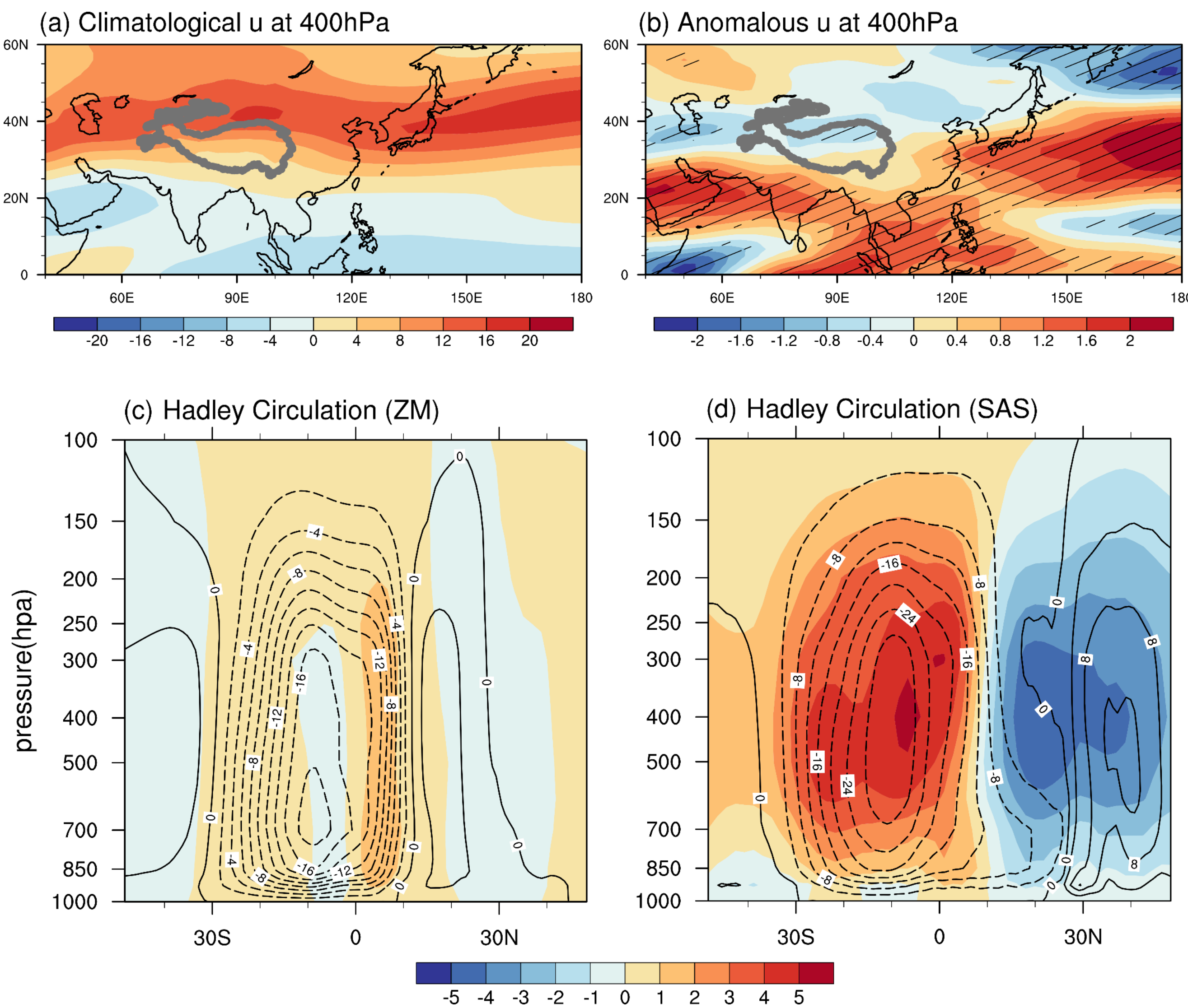

Fig. 10 (a) The climatological JJA mean zonal wind at 400 hPa (shading, m s^{-1}). (b) As in (a), but for the anomalies in the first JJA after tropical volcanic eruptions based on CESM-LME. Slashes and dots indicate values > 95% confidence level based on the Monte Carlo test (n = 10,000). Local Hadley circulation response (stream function response) during the first summer after tropical volcanic eruptions based on CESM-LME. (c) Local Hadley circulation computed in zonal mean and (d) in the South Asia monsoon domain (70–120°E). Shadings represent the anomalous circulation and contours refer to the pre-eruption 5 years climatology. Solid (dashed) lines represent positive (negative) values of the stream function for clockwise (counterclockwise) circulation (units: 10^{10} kg s^{-1})

underlying physical mechanisms. The major findings are summarized as following along with a schematic diagram of summer precipitation response over TP to tropical volcanic eruptions shown in Fig. 11.

1) Based on the instrumental data during the past decades and multiple precipitation reconstructions covering the past few centuries, we find a significant reduction in summer precipitation over the southern TP region during the first summer after tropical volcanic eruptions, decreased by over 1 mm day^{-1} on a regional scale, which is about 16.7% of climate mean value.
2) The summer precipitation responses to tropical volcanic eruptions are further confirmed based on the results from CESM-LME simulation. The SEA results show deficient rainfall over southern TP region, which is consistent with observations. A decrease of precipitation with an intensity of 1.2 mm day^{-1} is seen over the southwestern TP, accounts for ~ 14.6% of summer mean condition (Fig. 11).
3) We used the moisture and moist static energy budget analysis to reveal the underlying physical mechanisms based on model simulations. The results show that both the dynamic processes associated with atmospheric circulation changes and the thermodynamic processes

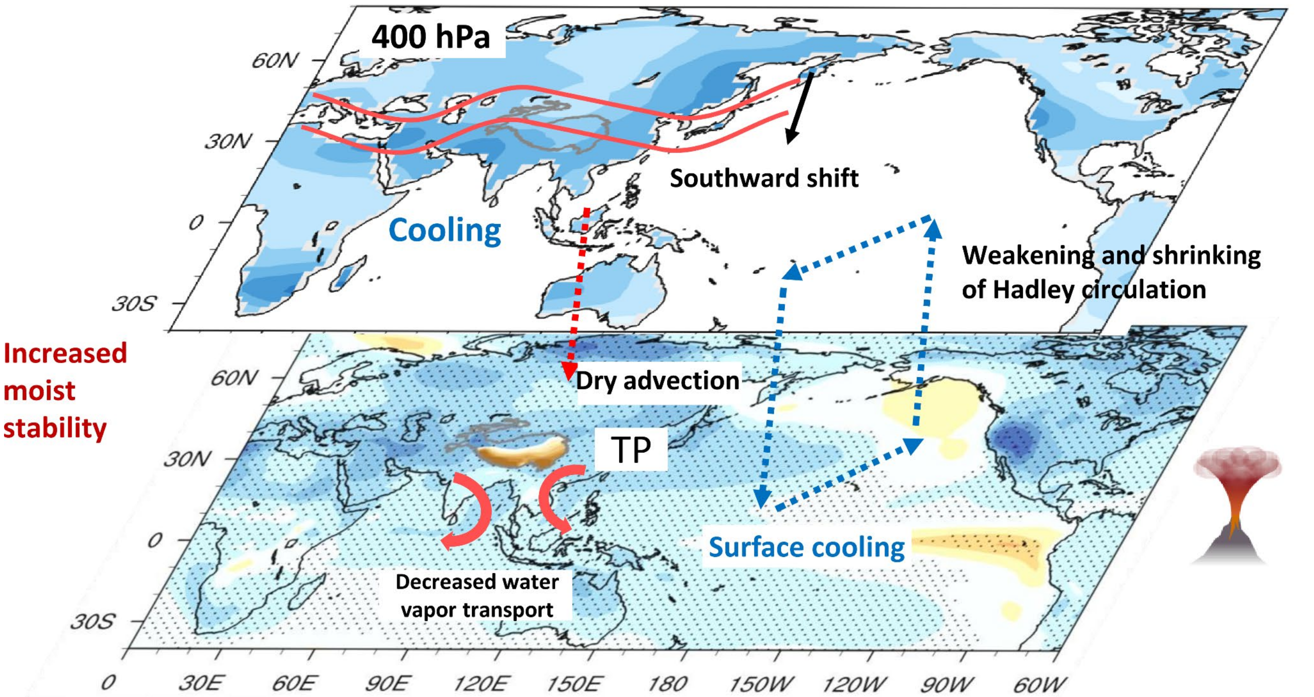

Fig. 11 Schematic diagram of the mechanism for summer precipitation responses over the Tibetan Plateau following large tropical volcanic eruptions. Negative precipitation anomalies are denoted by brown color. Shading represents temperature anomalies. Red vectors are low level wind anomalies. Red contours at 400 hPa represent the location of climatological westerly jet and response to volcanic eruptions, respectively. Blue dashed arrows denote changes in local Hadley circulation

associated with specific humidity changes contribute to the decreased precipitation in the SouthWest region of TP, while the changes in thermodynamic process dominates the reduction of precipitation in the South-East region of TP. The thermodynamic process results from decreased atmospheric precipitable water caused by decreased surface temperature after tropical volcanic eruptions, which reduce the water vapor transport to the southern TP region. The dynamic processes are caused by increased gross moist stability, stronger cooling over the west side of TP and a significant southward shift of westerlies after tropical eruptions (Fig. 11). The southward shift of westerlies is related to weakening and shrinking of Hadley circulation.

Our results imply that major tropical eruptions have significant impact on the summer precipitation over the southern TP regions, which will further decrease the source of supply for the “Asian water tower” glaciers and runoff output. The impacts of tropical eruptions on TP climate are needed to be considered in the design of geoengineering experiments. Potential volcanic eruptions are suggested to be included in the design of near-term decadal climate prediction experiments.

Acknowledgements We are grateful to the anonymous reviewers for their valuable and helpful suggestions.

Funding This work is jointly supported by the National Program on Key Basic Research Project of China (Grant No. 2017YFA0604601), the National Natural Science Foundation of China (Grants No. 41988101, 42105047), the National Program on Key Basic Research Project of China (Grant No. 2020YFA0608902), the Second Tibetan Plateau Scientific Expedition and Research (STEP) program (Grant No. 2019QZKK0102), and the Jiangsu Collaborative Innovation Center for Climate Change.

Data Availability The CESM-LME simulations were acquired from the website of Earth system grid (https://www.earthsystemgrid.org/dataset/ucar.cgd.ccsm4.CESM_CAM5_LME.html). The reconstructions were acquired from the website of NCDC (https://www.ncei.noaa.gov/access/paleo-search/). Other published sources of observational datasets for precipitation are cited in the main text.

Declarations

Conflict of interest The authors have no competing interests to declare that are relevant to the content of this article.

References

Acosta RP, Huber M (2017) The neglected Indo-Gangetic Plains low-level jet and its importance for moisture transport and precipitation during the peak summer monsoon. Geophys Res Lett 44(16):8601–8610

Adams JB, Mann ME, Ammann CM (2003) Proxy evidence for an El Nino-like response to volcanic forcing. Nature 426(6964):274–278

Anand A, Mishra SK, Sahany S, Bhowmick M, Rawat JS, Dash SK (2018) Indian Summer Monsoon Simulations: Usefulness of Increasing Horizontal Resolution, Manual Tuning, and Semi-Automatic Tuning in Reducing Present-Day Model Biases.Sci Rep8

Anchukaitis KJ, Buckley BM, Cook ER, Cook BI, D'Arrigo RD, Ammann CM (2010) Influence of volcanic eruptions on the climate of the Asian monsoon region. Geophys Res Lett 37(22):L22703

Annamalai H, Taguchi B, McCreary JP, Nagura M, Miyama T (2017) Systematic Errors in South Asian Monsoon Simulation: Importance of Equatorial Indian Ocean Processes. J Clim 30(20):8159–8178

Azoulay A, Schmidt H, Timmreck C (2021) The Arctic polar vortex response to volcanic forcing of different strengths. Journal of Geophysical Research: Atmospheres, 126(11), e2020JD034450

Back LE, Bretherton CS (2009) A Simple Model of Climatological Rainfall and Vertical Motion Patterns over the Tropical Oceans. J Clim 22(23):6477–6497

Barnes EA, Solomon S, Polvani LM (2016) Robust Wind and Precipitation Responses to the Mount Pinatubo Eruption, as Simulated in the CMIP5 Models. J Clim 29(13):4763–4778

Bollasina M, Nigam S (2009) Indian Ocean SST, evaporation, and precipitation during the South Asian summer monsoon in IPCC-AR4 coupled simulations. Clim Dyn 33(7–8):1017–1032

Bollasina MA, Ming Y (2013) The general circulation model precipitation bias over the southwestern equatorial Indian Ocean and its implications for simulating the South Asian monsoon. Clim Dyn 40(3–4):823–838

Boos WR, Hurley JV (2013) Thermodynamic Bias in the Multimodel Mean Boreal Summer Monsoon. J Clim 26(7):2279–2287

Chai J, Liu F, Xing C, Wang B, Gao C, Liu J, Chen D (2020) A robust equatorial Pacific westerly response to tropical volcanism in multiple models. Clim Dyn 55(11–12):3413–3429

Chou C, Neelin JD, Chen C-A, Tu J-Y (2009) Evaluating the "Rich-Get-Richer" Mechanism in Tropical Precipitation Change under Global Warming. J Clim 22(8):1982–2005

Cui X, Gao Y, Sun J (2014) The response of the East Asian summer monsoon to strong tropical volcanic eruptions. Adv Atmos Sci 31(6):1245–1255

D'Agostino R, Brown JR, Moise A, Nguyen H, Silva Dias PL, Jungclaus J (2020) Contrasting southern hemisphere monsoon response: MidHolocene orbital forcing versus future greenhouse gas-induced global warming. J Clim 33(22):9595–9613

D'Agostino R, Timmreck C (2022) Sensitivity of regional monsoons to idealised equatorial volcanic eruption of different sulfur emission strengths. https://doi.org/10.1088/1748-9326/ac62af. Environmental Research Letters https://iopscience.

Dogar MM, Sato T (2019) A Regional Climate Response of Middle Eastern, African, and South Asian Monsoon Regions to Explosive Volcanism and ENSO Forcing. J Geophys Res 124(14):7580–7598

Ding T, Zhou T, Chen X et al (2021) Enhanced Turbulent Heat Fluxes Improve Meiyu-Baiu Simulation in High-Resolution Atmospheric Models. J Adv Model Earth Syst 13:1–19. https://doi.org/10.1029/2020MS002430

Ding Y, Carton JA, Chepurin GA, Stenchikov G, Robock A, Sentman LT, Krasting JP (2014) Ocean response to volcanic eruptions in Coupled Model Intercomparison Project 5 simulations. J Geophys Research-Oceans 119(9):5622–5637

Duan A, Sun R, He J (2017) Impact of surface sensible heating over the Tibetan Plateau on the western Pacific subtropical high: A land-air-sea interaction perspective. Adv Atmos Sci 34(2):157–168

Duan A, Wang M, Lei Y, Cui Y (2013) Trends in Summer Rainfall over China Associated with the Tibetan Plateau Sensible Heat Source during 1980–2008. J Clim 26(1):261–275

Feng L, Zhou T (2012) Water vapor transport for summer precipitation over the Tibetan Plateau: Multidata set analysis.J Geophys Res117

Feng S, Hu Q, Wu Q, Mann ME (2013) A Gridded Reconstruction of Warm Season Precipitation for Asia Spanning the Past Half Millennium. J Clim 26(7):2192–2204

Fiedler S, Crueger T, D'Agostino R, Peters K, Becker T, Leutwyler D, Paccini L, Burdanowitz J, Buehler SA, Cortes AU, Dauhut T, Dommenget D, Fraedrich K, Jungandreas L, Maher N, Naumann AK, Rugenstein M, Sakradzija M, Schmidt H, Sielmann F, Stephan C, Timmreck C, Zhu X, Stevens B (2020) Simulated Tropical Precipitation Assessed across Three Major Phases of the Coupled Model Intercomparison Project (CMIP). Mon Wea Rev 148(9):3653–3680

Fischer EM, Luterbacher J, Zorita E, Tett SFB, Casty C, Wanner H (2007) European climate response to tropical volcanic eruptions over the last half millennium.Geophys Res Lett34 (5)

Gao C, Robock A, Ammann C (2008) Volcanic forcing of climate over the past 1500 years: An improved ice core-based index for climate models. J Geophys Res 113:D23

Grinsted A, Moore JC, Jevrejeva S (2007) Observational evidence for volcanic impact on sea level and the global water cycle. Proc Natl Acad Sci 104(50):19730–19734

Gu H, Yu Z, Peltier WR, Wang X (2020) Sensitivity studies and comprehensive evaluation of RegCM4.6.1 high-resolution climate simulations over the Tibetan Plateau. Clim Dyn 54(7–8):3781–3801

Haurwitz MW, Brier GW (1981) A Critique of the superposed epoch analysis method – its application to solar weather relations. Mon Wea Rev 109(10):2074–2079

Hersbach H, Bell B, Berrisford P, Hirahara S, Horanyi A, Munoz-Sabater J, Nicolas J, Peubey C, Radu R, Schepers D, Simmons A, Soci C, Abdalla S, Abellan X, Balsamo G, Bechtold P, Biavati G, Bidlot J, Bonavita M, De Chiara G, Dahlgren P, Dee D, Diamantakis M, Dragani R, Flemming J, Forbes R, Fuentes M, Geer A, Haimberger L, Healy S, Hogan RJ, Holm E, Janiskova M, Keeley S, Laloyaux P, Lopez P, Lupu C, Radnoti G, de Rosnay P, Rozum I, Vamborg F, Villaume S, Thepaut JN (2020) The ERA5 global reanalysis. Q J R Meteorol Soc 146(730):1999–2049

Huffman GJ, Adler RF, Bolvin DT, Gu G (2009) Improving the global precipitation record: GPCP Version 2.1.Geophys Res Lett36

Hurrell JW, Holland MM, Gent PR, Ghan S, Kay JE, Kushner PJ, Lamarque JF, Large WG, Lawrence D, Lindsay K, Lipscomb WH, Long MC, Mahowald N, Marsh DR, Neale RB, Rasch P, Vavrus S, Vertenstein M, Bader D, Collins WD, Hack JJ, Kiehl J, Marshall S (2013) The Community Earth System Model A Framework for Collaborative Research. Bull Amer Meteor Soc 94(9):1339–1360

Hu S, Zhou T, Wu B (2021) Impact of Developing ENSO on Tibetan Plateau Summer Rainfall. J Clim 34(9):3385–3400

Iles CE, Hegerl GC (2015) Systematic change in global patterns of streamflow following volcanic eruptions. Nat Geosci 8(11):838–842

Iles CE, Hegerl GC, Schurer AP, Zhang X (2013) The effect of volcanic eruptions on global precipitation. J Geophys Res 118(16):8770–8786

Immerzeel WW, van Beek LPH, Bierkens MFP (2010) Climate Change Will Affect the Asian Water Towers. Science 328(5984):1382–1385

Izumo T, Montegut CdB, Luo J-J, Behera SK, Masson S, Yamagata T (2008) The Role of the Western Arabian Sea Upwelling in Indian Monsoon Rainfall Variability. J Clim 21(21):5603–5623

Joshi IS (2010) Volcanic eruptions and their effects on soi, sst and indian summer monsoon rainfall. Disaster Adv 3(4):582–585

Levine RC, Turner AG (2012) Dependence of Indian monsoon rainfall on moisture fluxes across the Arabian Sea and the impact

of coupled model sea surface temperature biases. Clim Dyn 38(11–12):2167–2190
Li J, Yu R, Yuan W, Chen H, Sun W, Zhang Y (2015) Precipitation over East Asia simulated by NCAR CAM5 at different horizontal resolutions. J Adv Model Earth Syst 7(2):774–790
Li P, Furtado K, Zhou T, Chen H, Li J (2021) Convection-permitting modelling improves simulated precipitation over the central and eastern Tibetan Plateau. Q J R Meteorol Soc 147(734):341–362
Liang E, Dawadi B, Pederson N, Piao S, Zhu H, Sigdel SR, Chen D (2019) Strong link between large tropical volcanic eruptions and severe droughts prior to monsoon in the central Himalayas revealed by tree-ring records. Sci Bull 64(14):1018–1023
Liu F, Zhao T, Wang B, Liu J, Luo W (2018) Different Global Precipitation Responses to Solar, Volcanic, and Greenhouse Gas Forcings. J Geophys Res 123(8):4060–4072
Liu W, Shi F, Xiao G, Xue H, Duan A, Xiao C, Guo Z (2021) Impact of volcanic eruptions on hydro-thermal combination of the Tibetan Plateau and Arctic during mid-fifteenth Century. Quaternary Sci 41(3):714–725
Ma Y, Tang G, Long D, Yong B, Zhong L, Wan W, Hong Y (2016) Similarity and Error Intercomparison of the GPM and Its Predecessor-TRMM Multisatellite Precipitation Analysis Using the Best Available Hourly Gauge Network over the Tibetan Plateau. Remote Sensing 8 (7)
Maher N, McGregor S, England MH, Sen Gupta A (2015) Effects of volcanism on tropical variability. Geophys Res Lett 42(14):6024–6033
Man W, Zhou T (2014) Response of the East Asian summer monsoon to large volcanic eruptions during the last millennium. Chin Sci Bull 59(31):4123–4129
Neelin JD, Held IM, MODELING TROPICAL CONVERGENCE BASED ON THE MOIST STATIC ENERGY BUDGET (1987) Mon Wea Rev 115(1):3–12
O'Brien TA, Li F, Collins WD, Rauscher SA, Ringler TD, Taylor M, Hagos SM, Leung LR (2013) Observed Scaling in Clouds and Precipitation and Scale Incognizance in Regional to Global Atmospheric Models %J. J Clim 26(23):9313–9333
Otto-Bliesner BL, Brady EC, Fasullo J, Jahn A, Landrum L, Stevenson S, Rosenbloom N, Mai A, Strand G (2016) Climate Variability and Change since 850 CE: An Ensemble Approach with the Community Earth System Model. Bull Amer Meteor Soc 97(5):735–754
Paik S, Min S-K (2017) Climate responses to volcanic eruptions assessed from observations and CMIP5 multi-models. Clim Dyn 48(3–4):1017–1030
Pausata FSR, Camargo SJ (2019) Tropical cyclone activity affected by volcanically induced ITCZ shifts. Proc Natl Acad Sci 116(16):7732–7737
Peng Y, Shen C, Wang W-C, Xu Y (2010) Response of Summer Precipitation over Eastern China to Large Volcanic Eruptions. J Clim 23(3):818–824
Predybaylo E, Stenchikov GL, Wittenberg AT, Zeng F (2017) Impacts of a Pinatubo-size volcanic eruption on ENSO. J Geophys Res 122(2):925–947
Qiu J (2008) The third pole. Nature 454(7203):393–396
Schewe J, Heinke J, Gerten D, Haddeland I, Arnell NW, Clark DB, Dankers R, Eisner S, Fekete BM, Colon-Gonzalez FJ, Gosling SN, Kim H, Liu X, Masaki Y, Portmann FT, Satoh Y, Stacke T, Tang Q, Wada Y, Wisser D, Albrecht T, Frieler K, Piontek F, Warszawski L, Kabat P (2014) Multimodel assessment of water scarcity under climate change. Proc Natl Acad Sci 111 (9):3245-3250.
Robock A (2000) Volcanic eruptions and climate. Rev Geophys 38(2):191–219
Shi F, Zhao S, Guo Z, Goosse H, Yin Q (2017) Multi-proxy reconstructions of May-September precipitation field in China over the past 500 years. Clim Past 13(12):1919–1938
Shi H, Wang B, Cook ER, Liu J, Liu F (2018) Asian Summer Precipitation over the Past 544 Years Reconstructed by Merging Tree Rings and Historical Documentary Records. J Clim 31(19):7845–7861
Sperber KR, Annamalai H, Kang IS et al (2013) The Asian summer monsoon: An intercomparison of CMIP5 vs. CMIP3 simulations of the late 20th century. Clim Dyn 41:2711–2744. https://doi.org/10.1007/s00382-012-1607-6
Stevenson S, Otto-Bliesner B, Fasullo J, Brady E (2016) "El Niño Like" Hydroclimate Responses to Last Millennium Volcanic Eruptions. J Clim 29(8):2907–2921
Su F, Duan X, Chen D, Hao Z, Cuo L (2013) Evaluation of the Global Climate Models in the CMIP5 over the Tibetan Plateau. J Clim 26(10):3187–3208
Tan X, Ma Z, He K, Han X, Ji Q, He Y (2020) Evaluations on gridded precipitation products spanning more than half a century over the Tibetan Plateau and its surroundings. Journal of Hydrology 582.
Timmreck C (2012) Modeling the climatic effects of large explosive volcanic eruptions. Wiley Interdisciplinary Reviews-Climate Change 3(6):545–564
Tong K, Su F, Yang D, Zhang L, Hao Z (2014) Tibetan Plateau precipitation as depicted by gauge observations, reanalyses and satellite retrievals. Int J Climatol 34(2):265–285
Trenberth KE, Dai A (2007) Effects of Mount Pinatubo volcanic eruption on the hydrological cycle as an analog of geoengineering. Geophys Res Lett 34:15
Ueda H, Kamahori H, Yamazaki N (2003) Seasonal contrasting features of heat and moisture budgets between the eastern and western Tibetan plateau during the GAME IOP. J Clim 16(14):2309–2324
Ward B, Pausata FS, Maher N (2021) The sensitivity of the El Niño-Southern Oscillation to volcanic aerosol spatial distribution in the MPI Grand Ensemble. Earth Sys Dyn 12(3):975–996
Wang T, Zhao Y, Xu C, Ciais P, Liu D, Yang H, Piao S, Yao T (2021) Atmospheric dynamic constraints on Tibetan Plateau freshwater under Paris climate targets. Nature Climate Change 11 (3).
Wu B, Zhou T, Li T (2017) Atmospheric Dynamic and Thermodynamic Processes Driving the Western North Pacific Anomalous Anticyclone during El Nino. Part I: Maintenance Mechanisms. J Clim 30(23):9621–9635
Xie S-P, Xu H, Saji NH, Wang Y, Liu WT (2006) Role of narrow mountains in large-scale organization of Asian monsoon convection. J Clim 19(14):3420–3429
Xu X, Lu C, Shi X, Gao S (2008) World water tower: An atmospheric perspective.Geophys Res Lett35 (20)
Yao, T., Bolch, T., Chen, D. et al. (2022) The imbalance of the Asian water tower. Nat Rev Earth Environ. https://doi.org/10.1038/s43017-022-00299-4
Yang B, Qin C, Wang J, He M, Melvin TM, Osborn TJ, Briffa KR (2014) A 3,500-year tree-ring record of annual precipitation on the northeastern Tibetan Plateau. Proc Natl Acad Sci 111(8):2903–2908
Yao T, Pu J, Lu A, Wang Y, Yu W (2007) Recent glacial retreat and its impact on hydrological processes on the tibetan plateau, China, and sorrounding regions. Arct Antarct Alp Res 39(4):642–650
Yao T, Thompson L, Yang W, Yu W, Gao Y, Guo X, Yang X, Duan K, Zhao H, Xu B, Pu J, Lu A, Xiang Y, Kattel DB, Joswiak D (2012) Different glacier status with atmospheric circulations in Tibetan Plateau and surroundings. Nat Clim Change 2(9):663–667
Yao T, Xue Y, Chen D, Chen F, Thompson L, Cui P, Koike T, Lau WKM, Lettenmaier D, Mosbrugger V, Zhang R, Xu B, Dozier J, Gillespie T, Gu Y, Kang S, Piao S, Sugimoto S, Ueno K, Wang L, Wang W, Zhang F, Sheng Y, Guo W, Ailikun, Yang X, Ma Y, Shen SSP, Su Z, Chen F, Liang S, Liu Y, Singh VP, Yang K, Yang D, Zhao X, Qian Y, Zhang Y, Li Q (2019) Recent Third Pole's Rapid Warming Accompanies Cryospheric Melt and Water Cycle Intensification and Interactions between Monsoon and Environment:

Multidisciplinary Approach with Observations, Modeling, and Analysis. Bull Amer Meteor Soc 100(3):423–444

Yatagai A, Kamiguchi K, Arakawa O, Hamada A, Yasutomi N, Kitoh A (2012) APHRODITE Constructing a Long-Term Daily Gridded Precipitation Dataset for Asia Based on a Dense Network of Rain Gauges. Bull Amer Meteor Soc 93(9):1401–1415

Zhang L, Su F, Yang D, Hao Z, Tong K (2013) Discharge regime and simulation for the upstream of major rivers over Tibetan Plateau. J Geophys Res 118(15):8500–8518

Zhang G, Xie H, Yao T, Li H, Duan S (2014) Quantitative water resources assessment of Qinghai Lake basin using Snowmelt Runoff Model (SRM). Journal of Hydrology 519:976-987.

Zhu Y-Y, Yang S (2020) Evaluation of CMIP6 for historical temperature and precipitation over the Tibetan Plateau and its comparison with CMIP5. Adv Clim Change Res 11(3):239–251

Zhuo Z, Gao C, Pan Y (2014) Proxy evidence for China's monsoon precipitation response to volcanic aerosols over the past seven centuries. J Geophys Res 119(11):6638–6652

Zuo M, Man W, Zhou T, Guo Z (2018) Different Impacts of Northern, Tropical, and Southern Volcanic Eruptions on the Tropical Pacific SST in the Last Millennium. J Clim 31(17):6729–6744

Zuo M, Zhou T, Man W (2019) Hydroclimate Responses over Global Monsoon Regions Following Volcanic Eruptions at Different Latitudes. J Clim 32(14):4367–4385

Zuo M, Man W, Zhou T (2021) Dependence of Global Monsoon Response to Volcanic Eruptions on the Background Oceanic States. J Clim 34(20):8273–8289

Publisher's Note Springer Nature remains neutral with regard to jurisdictional claims in published maps and institutional affiliations.

Supplementary Information The online version contains supplementary material available at https://doi.org/10.1007/s00382-022-06463-2.